CONSTRUCTION OF THIRD-ORDER ENO AND WENO FINITE VOLUME SCHEMES FOR GENERIC UNSTRUCTURED GRIDS

William R. Wolf
Instituto Tecnológico de Aeronáutica, CTA-ITA, São José dos Campos, São Paulo, 12228-900, Brazil
will_wolf@yahoo.com

João Luiz F. Azevedo
Instituto de Aeronáutica e Espaço, CTA-IAE, São José dos Campos, São Paulo, 12228-904, Brazil
azevedo@iae.cta.br

Abstract. *In the present work, the essentially non-oscillatory schemes (ENO) and the weighted essentially non-oscillatory schemes (WENO) are implemented in a cell centered finite volume context on unstructured meshes. The meshes are composed by any type of polygonal control volume, such as triangles or quadrilaterals, and hybrid meshes can be also treated. The non-dimensional 2-D Euler equations are considered to represent the flows of interest. The ENO and WENO schemes have been developed with the purpose of accurately capturing discontinuities appearing in problems governed by hyperbolic conservation laws. In the aerodynamic studies of interest in the present paper, these discontinuities are mainly represented by shock waves and contact surfaces. The entire reconstruction process of ENO and WENO schemes is described in detail for any order of accuracy with an emphasis on the implementation of third-order scheme. Roe's flux difference splitting method is used to approximate flux values on the cell boundaries. TVD Runge-Kutta scheme is used to advance the solution of the governing equations in time. A multigrid method is used in the present work and applications for aerodynamic flows are presented comparing the accuracy of the schemes with data available in the literature.*

Keywords: *ENO, WENO, HIGH-ORDER SCHEMES, UNSTRUCTURED GRIDS*

1. Introduction

The motivation for the present work is the need for accurate simulations of high Mach number aerodynamic flows with strong discontinuities. In recent years several efforts have been made by the CFD group of Instituto de Aeronáutica e Espaço [3, 4, 5] for the development of computational tools which are able of accurately capturing discontinuities such as the shock waves appearing in the aerodynamic flows of interest. Some upwind schemes such as the van Leer flux vector splitting scheme [18], the Liou AUSM$^+$ flux vector splitting scheme [11] and the Roe flux difference splitting scheme [13] were implemented and tested for second-order accuracy considering a TVD-MUSCL reconstruction [2]. However, Azevedo *et al.* [4] shows that nominally second-order schemes presented results with an order of accuracy smaller than the expected in the solutions for unstructured grids. Aside from this fact, it is well known that TVD schemes have their order of accuracy reduced to first order in the presence of shocks due to the effect of limiters.

This observation initiated the development and implementation of essentially non-oscillatory (ENO) schemes, introduced by Harten *et al.* [8], in which oscillations up to the order of the truncation error are allowed to overcome the drawbacks and limitations of TVD schemes. Subsequent on the development of ENO schemes, the weighted essentially non-oscillatory (WENO) schemes were introduced by Liu *et al.* [12] with the purpose of presenting better convergence rate for stationary cases, better smoothing for the flux vectors and better accuracy using the same stencils as the ENO schemes.

In this work, the essentially non-oscillatory schemes (ENO) and the weighted essentially non-oscillatory schemes (WENO) are implemented in a cell centered finite volume context for unstructured meshes. The two dimensional Euler equations are considered to represent the flows of interest. The ENO and WENO schemes have been developed with the purpose of accurately capturing discontinuities appearing in problems governed by hyperbolic conservation laws. In the aerodynamic studies of interest in the present paper, these discontinuities are mainly represented by shock waves. The entire reconstruction process of ENO and WENO schemes is described in detail for quadratic polynomials and, hence, for third-order of accuracy of the numerical schemes, with extension to higher orders. Applications to aerodynamic flows are presented showing the accuracy of the schemes and their behavior. For the ENO schemes, interpolation polynomials of one order less than the order of accuracy expected in the solution are computed and these polynomials are used to reconstruct a good approximation to the values of the conserved variables within the cells. These polynomials interpolate primitive variable values in Gauss quadrature points using stencils determined by a von Neumann neighborhood [16]. The control volume moments and the mean values of primitive variables in the cells are used to compute the polynomial coefficients and, hence, one can compute the oscillation indicator of the polynomials and select the smoothest among them through the values of these coefficients.

While the ENO schemes use the smoothest polynomial, the WENO schemes use all ENO computed polynomials for

the stencils and, therefore, they construct one polynomial only. Non negative weights, which must add up to one, are computed for every polynomial through oscillation indicators and the WENO polynomial is constructed by the sum of all the ENO polynomials multiplied by the respective weights [6, 12]. The weights attributed to the polynomials can be of the order of accuracy desired in the solution if these polynomials are in the discontinuous regions of the mesh or they can be of order one if the polynomials are in the smooth regions of the flow. Classical computational fluid dynamics applications such as the flow in a channel with a forward-facing step and the transonic flow over a NACA0012 airfoil are presented with the aim of comparing the accuracy of the proposed methods. Such an assessment of the methods here implemented is achieved through the comparison of the present numerical results with data available in the literature.

2. Theoretical Formulation

In the present work, the 2-D Euler equations are solved in their integral form as

$$\frac{\partial}{\partial t}\int_V Q dV + \int_S (\vec{P}\cdot\vec{n}) dS = 0\,, \tag{1}$$

where V represents the control volume, S represents the surface of the control volume and $\vec{n}$ is the unit normal vector to the surface, S, positive outward. Q is the vector of conserved variables, and $\vec{P}$ represents the sum of the convective flux vectors. The system is closed by the equation of state for a perfect gas.

The control volumes considered in this work are triangles and quadrilaterals and they can be decomposed into a finite number of line segments Γ_j. One should observe that the control volumes could be composed by any type of polygon, because the really important aspect is that its bounding contour could be decomposed into a finite number of line segments. The surface integral from Eq. (1) can be discretized using N-point Gaussian integration formulae

$$\int_{S_i} (\vec{P}\cdot\vec{n}) dS \approx \sum_j |\Gamma_j| \sum_{\ell=1}^{N} w_\ell \vec{P}(Q(G_\ell), t)\cdot\vec{n}\,, \tag{2}$$

where G_ℓ and w_ℓ are, respectively, the Gaussian points and the weights on the Γ_j line segment. For the third-order schemes, two Gaussian points are necessary along each line segment. Their values are given by

$$G_1 = \frac{\sqrt{3}+1}{2\sqrt{3}} z_1 + (1 - \frac{\sqrt{3}+1}{2\sqrt{3}}) z_2 \quad \text{and} \quad G_2 = \frac{\sqrt{3}+1}{2\sqrt{3}} z_2 + (1 - \frac{\sqrt{3}+1}{2\sqrt{3}}) z_1, \tag{3}$$

and the respective weights, w_1 and w_2, are choosen as $w_1 = w_2 = 1/2$.

Using the method described above, one can compute values of Q_i in some instant, t, and then, from these mean values, one can reconstruct polynomials that represent the primitive variables ρ, u, v and p. Finally, it is possible to compute values of the conserved variables in the Gaussian points. Due to the discontinuity of the reconstructed values of the conserved variables over the cell boundaries, one must use a numerical flux function to approximate these flux values on the cell boundaries. In this work, the authors have used the Roe flux difference splitting method [13] to compute such approximations. A fully explicit third-order accurate TVD Runge-Kutta scheme was used to advance the solution of the governing equations in time, for the spatially third-order scheme, and this TVD Runge-Kutta scheme can be found in Shu and Osher [15].

3. ENO and WENO Reconstructions

3.1 General Considerations

The reconstruction procedure of the ENO schemes is based on the approximation of mean values of the primitive variables for each cell in the mesh by polynomials of one order less than the spatial order of accuracy expected. For the construction of polynomials of η-th order, one must use $N(\eta)$ cells, where $N(\eta) = (\eta+1)(\eta+2)/2$. The first step in obtaining the polynomial reconstruction for each cell is to define the possible set of cells, called a stencil, that will be used. In the finite volume cell centered scheme, the stencils can be selected in a von Neumann neighborhood for a linear polynomial reconstruction (second-order accuracy). This approach can be extended to higher orders through the use of von Neumann neighborhoods of the primary neighbors already selected for the second-order reconstruction. In the present work, the cells are triangles or quadrilaterals and the $p(x, y)$ polynomials can, then, be calculated as

$$p(x,y) = \sum_{|\beta|\le\eta} r_{\beta_1\beta_2} (x - x_c)^{\beta_1} (y - y_c)^{\beta_2}, \tag{4}$$

where $|\beta| = \beta_1 + \beta_2$, with $\beta_i \in \{0, 1, 2, \ldots\}$, x_c and y_c are the Cartesian coordinates of the barycenter of the control volumes and $r_{\beta_1\beta_2}$ are unknown coefficients which are some approximations to the derivatives of the primitive variables.

Once it is established that $p(x, y)$ is a good approximation to the mean values of primitive variables for each cell, one can write a linear system, $[R]\{r\} = \{\overline{u}\}$, of $N(\eta)$ equations for the $N(\eta)$ unknowns, $r_{\beta_1\beta_2}$. Here, $[R]$ is the matrix of control volume moments, as in Gooch [7], computed using the scaling technique proposed by Friedrich [6] to circumvent a poorly conditioned matrix. Moreover, $\{r\}$ is the vector of unknown coefficients that must be found and $\{\overline{u}\}$ is the vector composed by the mean values for each primitive variable. The stencil is considered admissible if the $[R]$ matrix is invertible. The control volume moments that compose the $[R]$ matrix are defined by Eq. (5) as

$$\overline{x^{\varphi}y^{\zeta}} \equiv \frac{1}{V_i}\int_{S_i}(x - x_c)^{\varphi}(y - y_c)^{\zeta}dS, \tag{5}$$

and are evaluated using Gauss quadrature formulae following the same procedure as the one used in the flux computation.

After the polynomial reconstruction is performed for each cell, the next step is to verify which polynomial is the least oscillatory to use in the ENO scheme. The oscillation is computed using some indicator that assesses the smoothness of $p(x, y)$. Following the results presented in the literature [6, 20], the oscillation indicator used in the present work is the one proposed by Jiang and Shu [10], which was later modified by Friedrich [6]. The formulation for this oscillation indicator can be expressed as

$$OI_{JS}(p(x,y)) = \left[\sum_{1\leq|\beta|\leq\eta}\int_{V_i} h^{2|\beta|-4}\left(\frac{\partial^{|\beta|}p(x,y)}{\partial x^{\beta 1}\partial y^{\beta 2}}\right)^2 dxdy\right]^{\frac{1}{2}}, \tag{6}$$

where h is the mesh width.

Differently from the ENO schemes, the WENO schemes use all the calculated polynomials. These polynomials are added together through the use of weights which are computed for each one of the polynomials as proportional to its respective oscillation indicator. The main idea in the WENO reconstruction is to attribute the computed weights for each polynomial with the aim of reconstructing a new polynomial as $p(x, y) = \sum_{k=1}^{m}\omega_k p_k(x, y)$. The weights are of order one in the smooth regions of the flow and are of the order of the desired accuracy in the solution in the regions with discontinuities. The weights can be computed as

$$\omega_k = \frac{[\epsilon + OI(p_k(x,y))]^{-\theta}}{\sum_{k'=1}^{m}[\epsilon + OI(p_{k'}(x,y))]^{-\theta}}, \tag{7}$$

where ϵ is a small real number used to avoid division by zero and θ is a positive integer. The WENO schemes have the property of being very smooth and stable in smooth regions of the flow, but this property is lost if θ is choosen too large. In that case the scheme tends to behave like the ENO schemes. In the present work, the θ term is choosen as $\theta = 2$ because this yielded the best convergence rates in the results.

3.2 Stencil Selection Algorithm

In Refs. [19] and [20], reconstruction of second-order accurate ENO and WENO schemes was presented. Details regarding to stencil selection algorithms were discussed and results appearing in these cited references comproved the accuracy of the second-order accurate ENO and WENO methods. For the implementation of the third-order accurate schemes one must use six cells for the polynomial reconstructions. Five unknown coefficients are computed for each polynomial through the solution of a five equation linear system composed by the control volume moments and the primitive variables of the cells considered in the stencil. The algorithm implemented in this work is based on the ideas proposed by Abgrall [1]. The first step consists in finding the stencil that presents the smoothest oscillation among the possible stencils for a linear reconstruction using only the primary neighbors of the main control volume. This algorithm uses this concept for both the ENO and WENO schemes for meshes composed by triangles and quadrilaterals. After the smoothest three-cell stencil is choosen, one must start the procedure for the third-order accuracy reconstruction. If the control volume is a triangle one has a maximum of 4 secondary neighbors for the reconstruction and, therefore, 4 possibilities of stencils for the selection. However, if the control volume is a quadrilateral, one has a maximum of 6 secondary neighbors for the reconstruction and, therefore, 20 possibilities of stencils for the selection. In Fig. 1 one can see a typical neighborhood for the implementation of the algorithm with the hatched volumes representing a possible stencil for this algorithm.

Althought the case where one has 20 stencils for the selection can occur, in most cases, one has 5 secondary neighbors for the reconstrucion in quadrilaterals and, then, 10 possibilities of stencils for the selection. Such a situation happens because, when selecting the stencil with the primary neighbors, one has, in most cases, a stencil that is not centered as can be viewed in Fig. 2 for the control volumes labeled NG1 and NG2. In such case, one can see that there are 5 secondary neighbors (the control volumes labeled as 2nd NG). In triangular control volumes, one can have the presence of three secondary neighbors for the reconstruction, which is the worst case for reconstruction on a triangular mesh. A case such this can be observed in Fig. 3, where the hatched control volumes NG1 and NG2 compose the smoothest stencil for a

second-order reconstruction and the hatched control volumes, NG3, NG4 and NG5, are the control volumes used for the third-order reconstruction. As one can see, this case allows the construction of only one stencil for the selection. If this stencil is in a discontinuous region of the flow, it will produce oscillations, and it will lead to a non-physical solution. Hence, the procedure adopted to avoid the problem where one has a stencil such this in a discontinuos region of the flow is to reduce the order of accuracy of the scheme in these cells.

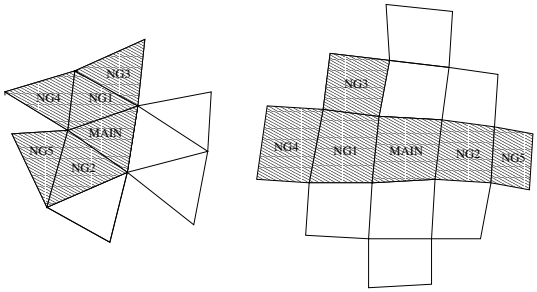

Figure 1. Typical neighborhood for a third-order accuracy reconstruction. The hatched volumes exemplify a possible stencil for the reconstruction.

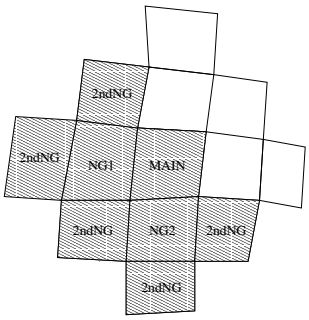

Figure 2. Neighborhood for a third-order accuracy reconstruction in a mesh composed exclusively by quadrilaterals. The 5 different hatched volumes marked as 2ndNG can compose only 10 stencils, instead of the 20 stencils that could be composed if the cells NG1 and NG2 were centered, as in Fig. 1.

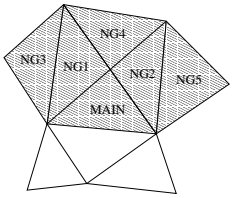

Figure 3. Possible stencil for a third-order accuracy reconstruction. The second-order stencil composed by the cells NG1 and NG2 was selected as the smoothest. Then, due to the lack of possibilities to switch the cells, one have to reduce the order of accuracy in cases where this stencil is in a discontinuous region of the flow.

The algorithm here implemented has presented good results for the most cases analyzed in the present work. As expected, the WENO schemes presented better results with respect to the convergence ratio and with respect to the smoothness of the solution in comparison with the ENO schemes. As mentioned in the papers of Abgrall [1] and Harten and Chakravarthy [9], one has to reduce the order of accuracy in some cells to maintain the stability of the schemes for both the ENO and the WENO schemes. The technique used for the reduction of the order of accuracy is the same presented by Abgrall [1].

4. Results

The present section discusses computational results for third-order schemes, which were formulated for meshes composed by triangles and quadrilaterals. The objective of the present study is to verify the newly implemented capability and to assess its advantages/disadvantages with regard to the discretization methods previously available in the code. Hence, the test cases here analyzed were selected among those for which well document, independent data are available in the

literature. A Full Approximation Storage (FAS) multigrid algorithm [17] is used for faster convergence to steady state solutions.

4.1 Forward-Facing Step

The first test case is a compressible flow in a channel with a forward-facing step that is well documented in the original paper of Woodward and Colella [21]. The channel lenght is 3, with height 1, in dimensionless units. The step is located in a position 0.6 dimensionless units from the channel entrance. It has a height of 0.2 dimensionless units. Two different meshes are used to test the schemes. The first mesh considered in this test case has 16384 nodes and 16064 quadrilateral control volumes, and the second mesh considered in this test case has 7022 nodes and 13608 triangular control volumes. An uniform Mach number of 3.0 is set as inflow at $t = 0$ dimensionless time units. Density was made dimensionless with respect to the entrance condition and pressure was made dimensionless with respect to the density times the speed of sound squared. One should observe that this test case is unsteady. The more interesting structure of the flow develops at time equal to $t = 4.0$ dimensionless time units. Results at this instant of time appear in Figs. 4 and 5, for the computation with WENO schemes. In Fig. 4 (a) one can see the solution for the second-order WENO scheme, and in Fig. 4 (b) one can see the solution for the third-order WENO scheme. The solutions presented in Figs. 4 (a) and (b) were obtained for the mesh composed exclusively by quadrilateral control volumes. In Fig. 5 (a) one can see the solution for the second-order WENO scheme, and in Fig. 5 (b) one can see the solution for the third-order WENO scheme. The solutions presented in Figs. 5 (a) and (b) were obtained for the mesh composed exclusively by triangular control volumes. The second-order WENO scheme analyzed in this test case used the second-order TVD Runge-Kutta scheme and the third-order WENO scheme used the third-order TVD Runge-kutta scheme. Roe's numerical flux function was used to evaluate the flux in the edges of the control volumes for all the schemes.

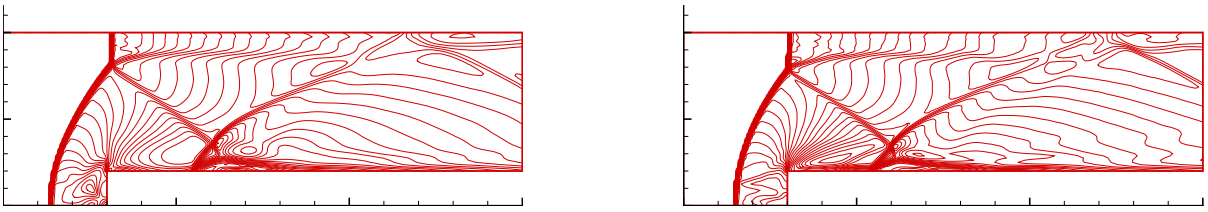

(a) Mach number contours for the second-order WENO scheme.

(b) Mach number contours for the third-order WENO scheme.

Figure 4. Mach number contours at t = 4.0 dimensionless time units for the quadrilateral mesh.

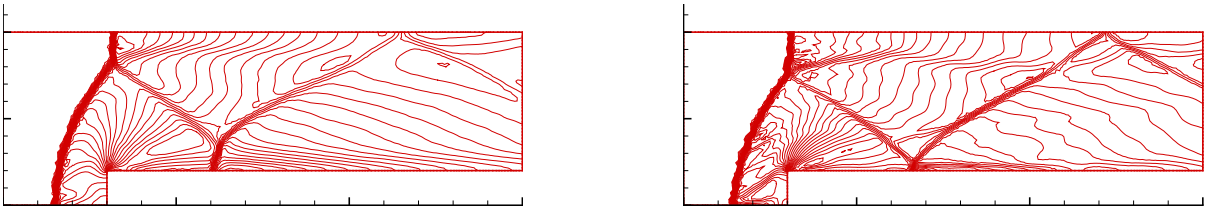

(a) Mach number contours for the second-order WENO scheme.

(b) Mach number contours for the third-order WENO scheme.

Figure 5. Mach number contours at t = 4.0 dimensionless time units for the triangular mesh.

At the instant of time presented in the solutions, a detached shock evolves to a lambda shock that reflects in the upper surface of the channel. A contact discontinuity is created past the lambda shock and both the reflected shock and the contact discontinuity move downstream along the channel. The reflected shock is again reflected at the lower wall as well as near the end of the channel. The contact discontinuity interacts with the shock that reflected in the lower wall. This interaction occurs in the region near the end of the channel, just upstream of the last reflection of the shock. At the corner region, there is also a weak oblique shock wave that ends the expansion region due to a Prandtl-Meyer expansion fan. This weak shock interacts with the first reflected shock near the lower wall of the channel. This leads typically to a flow structure that resembles an unphysical shock-boundary layer interaction in the region where the second shock reflection occurs. The solution in this region is very dependent on the treatment applied to the corner of the step. In the present work, no special treatment was applied to the corner of the step, contrary to the original reference [21]. One can see that the results here presented are similar to those presented in Refs. [1] and [16], where, as in this work, no special treatment was applied to the corner of the step.

The results obtained in Fig. 4 for the mesh composed by quadrilateral control volumes presented a very sharp capture

of the first detached shock and of the lambda shock that reflects in the upper wall of the channel. The contact discontinuity was also well captured for both second and third-order WENO schemes. The first reflection of the shock, as well as the second reflection, were well defined in the solutions for both schemes. For the quadrilateral mesh one can observe that the second reflection of the shock, in the lower wall, was affected by the unphysical shock-boundary layer created downstream of the corner region. This shock-boundary layer interaction is very pronounced for both WENO schemes here analyzed. One can see that the third-order WENO scheme captured the expansion fan as well as the weak compression shock near the corner region. The second-order WENO scheme was not able to capture such phenomena. In the post-shock region, in the lower wall of the channel, one can observe a separation bubble. This circulation zone appears only for the calculations with the quadrilateral mesh. The region where the contact discontinuity and the second shock reflection meet is better resolved by the third-order WENO scheme and the third reflection of the shock, near the end of the channel, is better captured by the third-order scheme.

The results obtained for the mesh composed by triangular control volumes presented a difference regarding with the height where the lambda shock is positioned. One can see that the lambda shock forms closer to the wall for the second-order WENO scheme and this affects the position of the contact discontinuity. In Fig. 5, one can see that all the shock reflections and the contact discontinuity are better captured for the third-order scheme. The second-order WENO scheme presented the shock-boundary layer interaction created past the corner region in the lower wall of the channel, although such effect is much less pronounced in this case than in the solutions with quadrilateral meshes. In other words, the second reflection of the shock presented a Y shock instead of a simple reflection in the wall. The results for the second-order scheme in the region where the interaction between the contact discontinuity and the last shock reflection occurs are poor in comparison with the third-order scheme results. The third-order WENO scheme captured the weak shock near the corner region very well, as in the results shown in Sonar [16]. This scheme was the only one that did not present any shock-boundary layer interaction-type phenomenon in the second shock reflection in the lower wall of the channel. All the shock reflections have a better resolution for the third-order WENO scheme and they are in the correct positions compared to Ref. [21].

4.2 NACA0012 Airfoil

The second test case considered here is the transonic flow over a NACA0012 airfoil with zero degree angle-of-attack. The freestream has a Mach number value of $M_\infty = 0.8$. Density was made dimensionless with respect to the freestream condition and pressure was made dimensionless with respect to the density times the speed of sound squared. This case was computed using an unstructured mesh with 4369 nodes and 8414 triangular control volumes. Two additional agglomerated grids were used in the multigrid computations for this case. This is a steady case and, here, the CFL number was set as a constant value. Therefore, differently from the previous unsteady computations in which the time step was set constant throughout the flowfield, the CFL number is kept constant through the flow in the present steady computation. Hence, one sets the CFL number and the local time step is computed using the local grid spacing and characteristic speeds. The numerical results for the pressure contours are plotted in Fig. 6 (a) for the third-order WENO scheme. For this case, both the ENO and the WENO schemes presented similar converged results for the third-order schemes. However, the WENO scheme presented a better convergence rate. The Cp distributions along the airfoil chord obtained with the second-order WENO scheme, the third-order WENO scheme, and for an experimental data obtained from Ref. [14] are plotted in Fig. 6 (b). The second-order method used the second-order TVD Runge-Kutta scheme for the temporal discretization while the third-order method used the third-order TVD Runge-Kutta scheme. All schemes considered Roe's method for numerical flux evaluation. In Fig. 6 (b), the black circles represent the experimental data found in Ref. [14], the red delta symbols represent the results for the second-order WENO scheme, and the blue squares represent the results obtained with the third-order WENO scheme.

Figure 6 (b) indicates that the third-order methods do a better job of capturing the shock wave over the airfoil, if compared to the second-order method. Moreover, there are oscillations in the leading-edge region of the airfoil for the second-order solution, which vanish for the third-order algorithm tested in this case. The sharper definition of the shock wave, obtained with the third-order method, is further emphasized by the reduced number of cells within the shock. The Cp distributions in the post-shock region again confirm the better resolution obtained with the third-order scheme. Finally, it is important to emphasize that the present computations are performed assuming inviscid flow. Nevertheless, the computational results are in good agreement with the available experimental data. One should observe, however, that the pressure rise across the shock wave, in the experimental results, is spread over a larger region due to the presence of the boundary layer and the consequent shock-boundary layer interaction that necessarily occurs in the experiment. For the numerical solution, the shock presents a sharper resolution, as one can expect for an Euler calculation.

5. Conclusions

The reconstruction of essentially non-oscillatory (ENO) schemes and weighted essentially non-oscillatory (WENO) schemes is presented in this work. An algorithm for third-order stencil selection is discussed for third-order ENO and

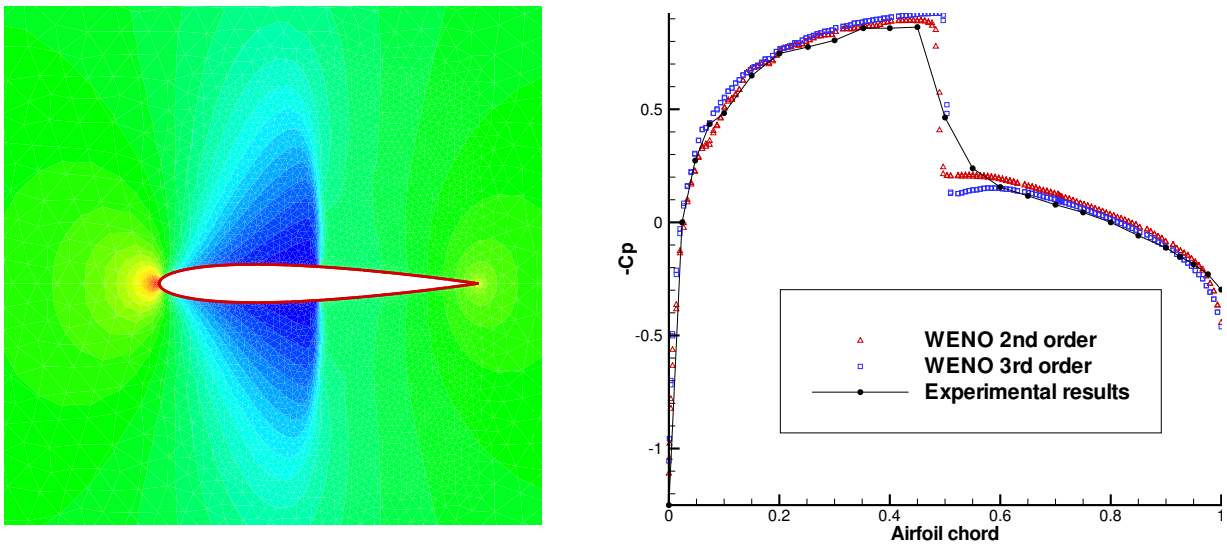

(a) Pressure contours over the NACA0012 airfoil in transonic flow.

(b) Cp distribution along the chord of the NACA0012 airfoil.

Figure 6. Transonic flow over a NACA0012 airfoil with zero degree angle-of-attack for freestream Mach number $M_\infty = 0.8$.

WENO schemes. Although, in this paper, only third-order accurate schemes are actually implemented and assessed, the formulation of ENO and WENO reconstruction is treated in a generic framework that allows the construction of polynomials of any order and, hence, of schemes with an arbitrary order of accuracy. The flux difference splitting scheme of Roe is used as the numerical flux function in the paper, and a third-order accurate TVD Runge-Kutta scheme is implemented to achieve the desired order of accuracy in the solutions. A multigrid method is used for faster convergence to steady state solutions..

6. Acknowledgments

The authors gratefully acknowledge the support of Fundação de Amparo à Pesquisa do Estado de São Paulo (FAPESP) through a Masters Scholarship for the first author under the FAPESP Grant No. 03/10047-2. The authors also acknowledge the partial support of Conselho Nacional de Desenvolvimento Científico e Tecnológico (CNPq) under the Integrated Project Research Grant No. 501200/2003-7. The authors are also thankful to Mr. Edson Basso for the very fruitful discussions during the course of the present research.

7. References

Abgrall, R., 1994, "On Essentially Non-Oscillatory Schemes on Unstructured Meshes: Analysis and Implementation," Journal of Computational Physics, Vol. 114, No. 1, pp. 45-58.

Anderson, W. K., Thomas, J. L., and van Leer, B., "A Comparison of Finite Volume Flux Vector Splittings for the Euler Equations," *AIAA Journal*, Vol. 24, No. 9, Sept. 1986, pp. 1453-1460.

Azevedo, J. L. F., and Korzenowski, H., 1998, "Comparison of Unstructured Grid Finite Volume Methods for Cold Gas Hypersonic Flow Simulations," AIAA Paper No. 98-2629, Proceedings of the 16th AIAA Applied Aerodynamics Conference, Albuquerque, New Mexico, pp. 447-463.

Azevedo, J. L. F., Figueira da Silva, L. F., and Strauss, D., 2005, "Order of Accuracy Study of Unstructured Grid Finite Volume Upwind Schemes," Paper submitted to the Journal of the Brazilian Society of Mechanical Sciences and Engineering.

Figueira da Silva, L. F., Azevedo, J. L. F., and Korzenowski, H., 2000, "Unstructured Adaptive Grid Flow Simulations of Inert and Reactive Gas Mixtures," Journal of Computational Physics, Vol. 160, No 2, pp. 522-540.

Friedrich, O., 1998, "Weighted Essentially Non-Oscillatory Schemes for the Interpolation of Mean Values on Unstructured Grids," Journal of Computational Physics, Vol. 144, No. 1, pp. 194-212.

Gooch, C. F. O., 1997, "High Order ENO Schemes for Unstructured Meshes Based on Least-Squares Reconstruction," Argonne National Laboratory, Report No. P631-1296, Mathematics and Computer Science Division.

Harten, A., Osher, S., Engquist, B., and Chakravarthy, S. R., 1987, "Uniformly High-Order Accurate Essentially Non-Oscillatory Schemes III," Journal of Computational Physics, Vol. 71, No. 2, pp. 231-303.

Harten, A., and Chakravarthy, S. R., 1991, "Multi-Dimensional ENO Schemes for General Geometries," ICASE Report No. 91-76.

Jiang, G. S., and Shu, C. W., 1996, "Efficient Implementation of Weighted ENO Schemes," Journal of Computational Physics, Vol. 126, No. 1, pp. 77-99.

Liou, M. S., 1996, "A Sequel to AUSM:AUSM+," Journal of Computational Physics, Vol. 129, No. 2, pp. 364-382.

Liu, X. D., Osher, S., and Chan, T., 1994, "Weighted Essentially Non-Oscillatory Schemes," Journal of Computational Physics, Vol. 115, No. 1, pp. 200-212.

Roe, P. L., 1981, "Approximatte Riemann Solvers, Parameter Vectors, and Difference Schemes," Journal of Computational Physics, Vol. 43, No. 2, pp. 200-212.

Scalabrin, L. C., 2002, "Numerical Simulation of Three-Dimensional Flows Over Aerospace Configurations," Master Thesis, Instituto Tecnológico de Aeronáutica, São José dos Campos.

Shu, C. W., and Osher, S., 1988, "Efficient Implementation of Essentially Non-Oscillatory Shock-Capturing Schemes," Journal of Computational Physics, Vol. 77, No. 2, pp. 439-471.

Sonar, T., 1997, "On the Construction of Essentially Non-Oscillatory Finite Volume Approximations to Hyperbolic Conservation Laws on General Triangulations: Polynomial Recovery, Accuracy and Stencil Selection," Comput. Methods Appl. Mech. Engr., Vol. 140, No. 2, pp. 157-181.

Strauss, D., 2001, "An Unstructured Grid Approach to the Solution of Axisymmetric Launch Vehicle Flows," Master Thesis, Instituto Tecnológico de Aeronáutica, São José dos Campos.

van Leer, B., 1982, "Flux-Vector Splitting for the Euler Equations," Proceedings of the 8th International Conference on Numerical Methods in Fluid Dynamics, Lecture Notes in Physics, Vol. 170, Springer-Verlag, Berlin, pp. 507-512.

Wolf, W. R., and Azevedo, J. L. F., 2004, "Implementation of ENO and WENO Schemes for Finite Volume Unstructured Grid Solutions of Compressible Aerodynamic Flows," ENCIT Paper No. 04-0048, Proceedings of the 10th Brazilian Congress of Thermal Sciences and Engineering (CD-ROM), Rio de Janeiro, RJ.

Wolf, W. R., and Azevedo, J. L. F., 2005, "High-Order Unstructured Grid ENO and WENO Schemes Applied to Aerodynamic Flows," AIAA Paper No. 2005-5115, Proceedings of the 17th AIAA Coputational Fluid Dynamics Conference (CD-ROM), Toronto, Canada.

Woodward, P., and Colella, P., 1984, "The Numerical Simulation of Two Dimensional Fluid Flow with Strong Shocks," Journal of Computational Physics, Vol. 54, No. 1, pp. 115-173.